

RESEARCH

Open Access



Extracellular vesicle miR-32 derived from macrophage promotes arterial calcification in mice with type 2 diabetes via inhibiting VSMC autophagy

Jingsong Cao^{1†} , Cong Chen^{2†}, Qian Chen^{1†}, Yan Gao¹, Zhibo Zhao¹, Qing Yuan¹, Anqi Li¹, Shiqi Yang¹, Yuqi He², Xuyu Zu^{3*} and Jianghua Liu^{1*}

Abstract

Background: The development of diabetes vascular calcification (VC) is tightly associated with the inhibition of vascular smooth muscle cell (VSMC) autophagy. Previously, our team found that miR-32-5p (miR-32) promotes macrophage activation, and miR-32 is expressed at higher level in the plasma of patients with coronary calcification. However, whether miR-32 mediates the function of macrophages in type 2 diabetes (T2D) VC is still unclear.

Methods: Wild-type (WT) and miR-32^{-/-} mice were used in this study. qRT-PCR and western blotting were used to analyze gene expression. Flow cytometry was used to analyze the influence of glucose concentration on macrophage polarization. Nanoparticle tracking analysis (NTA), transmission electron microscopy, and confocal microscopy were used to identify macrophage extracellular vehicles (EVs). Immunofluorescence, in situ hybridization (ISH), immunohistochemistry, and alizarin red staining were used to analyze the influence of macrophage EVs on autophagy and calcification of the aorta of miR-32^{-/-} mice. A luciferase assay was used to analyze the effect of miR-32 on myocyte enhancer factor 2D (Mef2d) expression. Co-IP combined with mass spectrometry (MS) and transcriptome sequencing was used to analyze the signalling pathway by which Mef2d acts in VSMC autophagy.

Results: We found that high glucose conditions upregulate miR-32 expression in macrophages and their EVs. Importantly, macrophages and their EVs promote VSMC osteogenic differentiation and upregulate miR-32 expression in VSMCs. Moreover, miR-32 mimics transfection promoted osteogenic differentiation and inhibited autophagy in VSMCs. In vitro and in vivo experiments showed that Mef2d is the key target gene of miR-32 that inhibits VSMC autophagy. Furthermore, MS and transcriptome sequencing found that cGMP-PKG is an important signalling pathway by which Mef2d regulates VSMC autophagy. In addition, after T2D miR-32^{-/-} mice were injected with macrophage

[†]Jingsong Cao, Cong Chen, and Qian Chen are contributed equally to this work.

*Correspondence: zuxuyu0108@hotmail.com; jianghua990@126.com

¹The First Affiliated Hospital, Institute of Clinical Medicine, Department of Endocrinology and Metabolism, Hengyang Medical School, University of South China, Hengyang 421000, Hunan, China

³The First Affiliated Hospital, Institute of Clinical Medicine, Department of Tumor Research, Hengyang Medical School, University of South China, Hengyang 421000, China

Full list of author information is available at the end of the article



EVs via the caudal vein, miR-32 was detected in aortic VSMCs of miR-32^{-/-} mice. Moreover, autophagy was significantly inhibited, and calcification was significantly enhanced in aorta cells.

Conclusions: These results reveal that EVs are the key pathway by which macrophages promote T2D VC, and that EVs miR-32 is a key cause of autophagy inhibition in VSMCs.

Keywords: Macrophage, EVs, miR-32, Diabetes, Vascular calcification

Introduction

Diabetes easily induces microvascular and macrovascular complications that lead to peripheral vascular disease [1]. Vascular calcification (VC) is an important clinicopathological feature of diabetes and is considered as a major independent risk factor for cardiovascular diseases [2]. In the process of VC, at least 4 kinds of cells may lead to VC. These cell types include pericytes in microvessels, pericyte-like calcifying vascular cells in the aortic intima, smooth muscle cells (SMCs) in the media, and myofibroblasts in the adventitia [3]. Among the 4 cell types, local smooth muscle cells are an important source of calcifying vascular cells [3–5]. The key to VSMC calcification is the transformation from a contractile phenotype to an osteoblast-like phenotype [6]. However, the mechanism of VSMC calcification is still unclear.

Our previous research determined that the expression of miR-32 is increased in VSMCs during the progression of vascular calcification, and miR-32 was expressed at high level in the plasma of VC patients compared with non-VC patients [7]. Interestingly, we further found that miR-32 is also involved in the activation of microglia, which are resident macrophages in the central nervous system [8]. Therefore, exploring the relationship and mechanisms among macrophages, miR-32 and VSMC calcification is meaningful.

Macrophages are the major participators of innate immunity and exist in all human tissues, including the aortic wall [9]. In response to infection, peripheral monocytes, derived from the bone marrow, are the major source of macrophages in the aortic wall [10]. In the plaques of human and mouse models, macrophages are abundant immune cells, and they are the primary cell type among total plaque cells [11, 12]. Infiltrated macrophages polarize to the proinflammatory M1 phenotype and secrete inflammatory factors and exosomes, leading to increased plaque stability [13, 14]. Macrophage polarization is a response to environmental stimulation and involves coordinated metabolic and transcriptional rewiring [15]. In diabetes, high glucose induces M1 macrophage polarization and the secretion of exosomes to regulate the development of cardiovascular diseases [16, 17]. Recent research found that the exosomes recovered by centrifugation include

oncosomes, ectosomes, microvesicles and membrane vesicles, so the production is better called EVs [18]. However, the roles of macrophages in T2D VC and how miR-32 increases in VSMCs are still unclear.

Autophagy is a catabolic process in cells that occurs via the lysosomal degradation pathway [9]. In the autophagy pathway, phagophore formation is a vital step in the formation of autophagosomes [19]. This process is regulated by several autophagy-related (Atg) proteins, including Beclin1 (Becn-1), Atg6 and Atg38 [20]. Following the development of autophagosomes, Atg proteins (e.g., Atg5, Atg16l1 and Atg7) also regulate their expansion and maturation of autophagosomes [21], while other proteins (e.g., sequestosome 1 (p62)) mediate autophagosome engulfment by lysosomes [22]. Diabetes mellitus is a chronic heterogeneous metabolic disorder [23]. Impaired autophagy mediates VSMC phenotypic conversion [24] and further accelerates VSMC calcification [25]. Clinically, insufficient autophagy activation is considered as one phenotypic feature of calcific aortic valve stenosis [26]. These results suggest that autophagy is closely associated with macrophage polarization and VC.

Therefore, this study aims to explore the mechanism by which macrophages promote VC in T2D. To address this aim, we found that miR-32 promotes M1 macrophage polarization under high glucose conditions and demonstrated that the secretion of EVs miR-32 is the major pathway by which macrophages promote VC in T2D through Mef2d/cGMP-PKG-mediated VSMC autophagy. Then, we verified the results in a T2D miR-32^{-/-} mouse model. These findings illustrate an important mechanism by which macrophages promote VC in T2D and identify a candidate biomarker of T2D VC.

Materials and methods

Cell lines culture

RAW264.7 and 293 T cells were purchased from the National Infrastructure of Cell Line Resource (China Center for Type Culture Collection) and were cultured in high- or low-glucose Dulbecco's modified Eagle's medium (DMEM, Gibco BRL, Grand Island, USA) with 10% fetal calf serum (FBS, Gibco, Australia) and 100 U/ml penicillin–streptomycin at 37 °C and 5% CO₂.

Mouse VSMCs separation and culture

Aortas were obtained from 8 to 10-week-old mice. Extravascular fat was removed from the aortas, and the aortas were cut open along the vessel lumen. Then, the tunica adventitia and endothelium of the vascular wall were removed. After cutting the aortas into small pieces, 1 ml culture medium (DMEM with 15% FBS and 1% penicillin–streptomycin) was added, and the sample was centrifuged at 250 g for 1 min. The precipitate was resuspended in 2 ml culture medium and transplanted into a T25 bottle (2 mice/bottle). After culturing at 37 °C and 5% CO₂ overnight, 2 ml culture medium was added, and the culture media was changed every 2 days. Finally, VSMCs were collected for further culture or analysis.

Macrophage EVs assay

EVs extraction from cell culture media was performed using a Total Exosome Isolation Reagent Kit (Thermo Fisher Scientific Inc., Waltham, MA USA) with some modifications. The dish with 70–80% confluent RAW264.7 cells was washed with 1 × PBS 3 times, serum-free medium was added, and the cells were cultured at 37 °C and 5% CO₂ for 24 h. The medium was subsequently collected and centrifuged at 2000 g for 30 min followed by 10,000 g for 30 min. Then, the supernatant was collected and incubated with a half volume of EVs isolation reagent at 4 °C overnight. Finally, the mixture was centrifuged at 10,000 g for 1 h, and the precipitate was resuspended in PBS. EVs were detected using nanoparticle tracking analysis (NTA), transmission electron microscopy and western blotting or were stored at –80 °C.

For the *in vitro* experiment, VSMCs were treated with EVs at a ratio of 1:1,000 and cultured at 37 °C and 5.0% CO₂ for 48 h. For the *in vivo* experiment, T2D mice were injected with 1.0×10^9 EVs via the tail vein once per week for two weeks.

Generation of T2D mice

8- to 10-week-old mice (C57/BL6 background) were fed a chow fat diet (CFD) or a high-fat diet (HFD) with 10% (TP23102) or 45% (TP 23100) of the energy from fat, respectively (Trophic Animal Feed High-tech Co., Ltd., Jiangsu, China). Five weeks later, an intraperitoneal insulin tolerance test (IPITT) assay was performed to detect changes in blood glucose after insulin (Sigma Chemical, USA) injection at 0, 15, 30, 60 and 120 min. Then, streptozotocin (STZ, Sigma Chemical, USA) was intraperitoneally injected at 25 mg/kg for 3 consecutive days. Blood glucose was measured from tail bleeds using a glucometer (Sannuo Biosensing Co., Ltd., Hunan, China)

at specified time points every week, and HFD-fed mice with blood glucose ≥ 11.1 mM or significantly higher than CFD-fed mice were considered to have T2D. Serum insulin was detected using a Mouse INS ELISA Kit (Feiya Biotechnology Co., Ltd., China). The Homeostasis Model Assessment–Insulin Resistance (HOMA-IR) index was calculated according to the formula $\text{HOMA-IR} = \text{Fasting blood glucose (mg/dL)} \times \text{fasting serum insulin (mU/mL)} / 405$.

Transwell assay

The influence of macrophages on VSMCs was assessed using Transwell plates (Corning Incorporated, NY, USA) containing a 0.4 μm pore membrane. RAW264.7 cells (1×10^5) were plated into the upper chamber, and equal numbers of VSMCs were plated into the lower surface. After culturing at 37 °C and 5.0% CO₂ for 48 h, VSMCs were collected for further analysis. Otherwise, the RAW 264.7 upper chamber was first treated with 1 μM 3,3'-di-octadecyloxycarbocyanine perchlorate (Dio) (MedChemExpress, NJ, USA) for 30 min or Dio for 30 min and 1 μM GW4869 (MedChemExpress) for 1 h, washed 3 times with culture medium and cocultured with VSMCs at 37 °C and 5.0% CO₂ for 48 h.

Transcriptome sequencing

VSMC was cocultured with or without RAW264.7 through 6-well transwell plates. After culturing at 37 °C and 5.0% CO₂ for 48 h, VSMC was collected and then analyzed via transcriptome sequencing by RiboBio (Guangzhou, China). Simply, after assessed the quantity integrity of RNA yield with K5500 (Beijing Kaiao Technology Development Co., Ltd, Beijing, China) and the Agilent 2200 Tape Station (Agilent Technologies, CA, USA) separately, the mRNA was treated according the requirements of Illumina. The purified library products were evaluated using the Agilent 2200 TapeStation and Qubit (Thermo Fisher Scientific). The libraries were sequenced by Illumina (Illumina, CA, USA). Raw fastq sequences were treated with Trimmomatic tools (v 0.36) using the following options: TRAILING:20, SLIDINGWINDOW:4:15 MINLEN:52, to remove trailing sequences below a phred quality score of 20 and to achieve uniform sequence lengths for downstream clustering processes. Sequencing read quality was inspected using the FastQC software. Adapter removal and read trimming were performed using Trimmomatic. Sequencing reads were trimmed from the end (base quality less than Q20) and filtered by length (less than 52).

Paired-end reads were aligned to the mouse reference genome mm10/hg19/rn6 with HISAT2. HTSeq v0.12.4 was used to count the reads numbers mapped to each gene.

MS analysis of MEF2D interaction protein

RAW264.7 was cultured in high-glucose condition. To remove nonspecific combination proteins, 1 ml of macrophage protein extract was incubated with 100 μ l of Protein A/G Plus Agarose (Santa Cruz Biotechnology, Inc., CA, USA), which had been washed twice and resuspended at a 50% concentration in PBS. After detecting the protein concentration, 2 μ g rabbit anti-mouse Mef2d antibody was added to 500 μ g protein extract, gently mixed by hand and then incubated overnight at 4 °C. On the second day, 50 μ l agarose at a 50% concentration was added and incubated at 4 °C for 2 h, followed by concentration at 800 g for 5 s. Finally, the agarose was collected and then identified via MS by BGI. Simply, the sample protein was separated by SDS-PAGE, and followed in gel digestion. 1/3 of total peptides were separated and analyzed with a nanoUPLC (EASYnLC1200) coupled to a Q Exactive HFX Orbitrap instrument (Thermo Fisher Scientific) with a nano electrospray ion source. Vendor's raw MS files were processed using MaxQuant software (Version 1.6.15.0) on a linux OS server (debian9).

The Antibodies information was showed in Table 2.

Hematoxylin and eosin (HE) analysis

Five randomly selected mice per group were subjected to deep anesthesia using 10% chloral hydrate (3.5 ml/kg, I.P.) and the tissues were extracted and fixed in 4% paraformaldehyde. Following fixation in paraffin, the tissues were cut into consecutive 4 μ m thick sections on a microtome, and the paraffin sections were transferred to poly-L-lysine-coated slides. The paraffin sections were processed in turn as baked at 60 °C for 12 h, incubated in xylene (Sinopharm, Shanghai, China) 3 times for 20 min, alcoholic (Sinopharm) gradient treated (100%, 95%, 85% and 75%) for 5 min per gradient, and soaked in double distilled water (ddH₂O) for 5 min. Then, the sections were used for further detection as follows.

HE staining was performed for the histopathological examination. The sections were processed in turn for hematoxylin staining for 1 min using ddH₂O washes, eosin staining for 30 s with ddH₂O washes, alcoholic gradient dehydration (95–100%) for 5 min per gradient, and incubated in xylene 2 times for 10 min. The sections were then exposed to a neutral resin (Sinopharm) sealing sheet and observed using a DAB kit (ZSGB-BIO).

Immunohistochemistry analysis

Deparaffinated sections of the aorta were prepared by heating the sample for 20 min, cooling the sample at

room temperature, and then washing the sample 3 times with 0.01 M PBS (pH 7.2–7.6) for 3 min. Endogenous peroxidase activity was blocked by incubating the sections in 1.0% periodic acid for 10 min and then washing them 3 times with 0.01 M PBS for 3 min. The sections were incubated with rabbit anti-mouse iNOS at 4 °C overnight. After the sections were washed 3 times with PBS for 5 min, they were incubated with anti-rabbit IgG-HRP at 37 °C for 30 min. They were then washed 3 times with PBS for 5 min, and further treated with Metal Enhanced DAB Substrate Kit (Solarbio) at room temperature for 1–5 min. Following hematoxylin staining, alcoholic dehydration, xylene treatment and application of a neutral resin sealing sheet, the sections were visualized using a DAB kit (ZSGB-BIO). The antibodies information was showed in Table 2.

In situ hybridization (ISH)

The experiment was carried out with mmu-miR-32-5p ISH Detection kit I (Boster, Wuhan, China). Simply, Deparaffinated sections of the aorta were prepared by heating the sample for 20 min, followed inactivation of endogenous enzymes 3% H₂O₂ at room temperature for 10 min. Then, the sections incubated with 3% citric acid-diluted pepsin at 37 °C for 15 min, treated with 1% paraformaldehyde at room temperature for 5 min, pre-hybridized with prehybridization liquid at 42 °C for 4 h, hybridized with hybridization liquid at 42 °C for overnight, blocking at 37 °C for 30 min, incubated with biotinylated rats' anti-digoxin at 37 °C for 1 h, treated with SABC at 37 °C for 20 min, incubated with biotinylated peroxidase at 37 °C for 20 min. Finally, the sections were visualized using a DAB kit (ZSGB-BIO) and stained with hematoxylin.

Immunofluorescence analysis

Deparaffinated aortic sections were prepared as follows: infiltrated in EDTA buffer (pH 9.0) and heated for 24 min, cooled to room temperature and washed 3 times with 0.01 M PBS (pH 7.2–7.6) for 3 min, infiltrated in sodium borohydride for 30 min with ddH₂O washes for 5 min, infiltrated in 75% alcohol for 30 s, stained Sudan black for 15 min with ddH₂O washes for 5 min, blocked in 10% FBS for 60 min, incubated with mouse p62 monoclonal antibody or rabbit anti-mouse LC3 antibody at 4 °C for overnight with PBS washes 3 times for 5 min each, incubated with anti-rabbit IgG conjugated CoraLite488 or anti-rat IgG conjugated CoraLite594 at 37 °C for 1 h, washed 5 min with PBS for 3 times and DAPI stained at 37 °C for 10 min. After washing with PBS and applying the glycerin sealing sheet, the sections were visualized using an inverted fluorescence microscope (OLYMPUS IX71). The antibodies information was showed in Table 2.

Identification of aorta calcification

Deparaffinated sections of the aorta were fixed in 95% alcohol for 15 min, and washed with 0.01 M PBS (pH 7.2–7.6) 3 times. The sections were stained with 50 μ l Alizarin Red S solution (Solarbio) for 5 min and then washed with ddH₂O for 3 times. After baking at 60 $^{\circ}$ C for 30 min and incubating in xylene 2 times for 10 min each, the sections were sealed with neutral resin (Sinopharm) sealing sheet and visualized using a DAB kit (ZSGB-BIO).

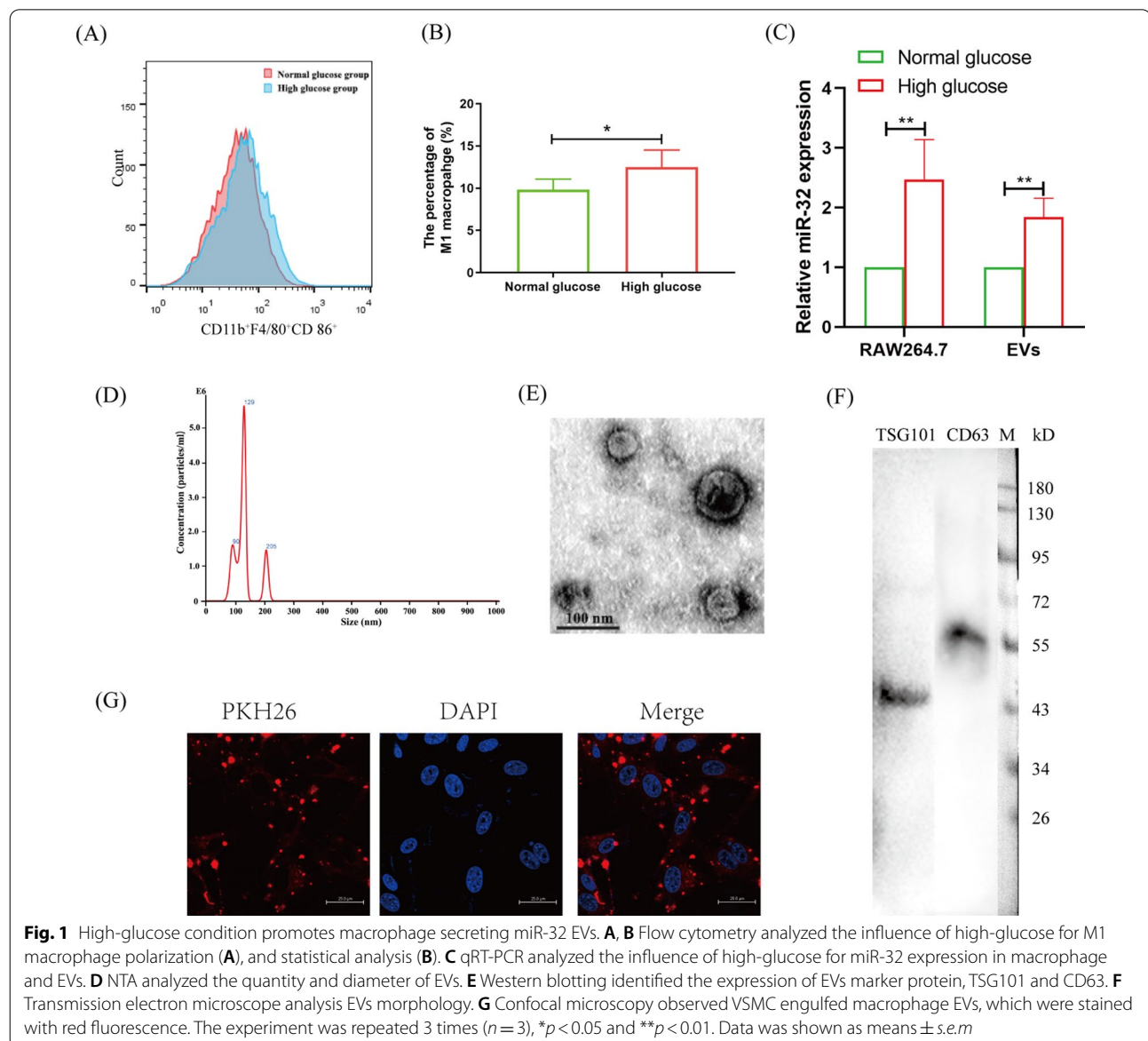
Transfection

After the cells reached 70% confluence, transfection mixture (100 μ l DMEM, 2 μ l Lipofectamine 3000 (Thermo),

25 nmol miR-32 mimics or 25 nmol miR-32 inhibitor or 12 pmol si-Mef2d or 1 μ g pDoubleEx-EGFP-Mef2d recombinant plasmid) was added to every 1 ml culture media, which was preincubated at room temperature for 20 min. The treated cells were cultured at 37 $^{\circ}$ C and 5% CO₂ for 24 h or 48 h.

Luciferase assay

The wild-type and mutant sequences of the 3' untranslated region (UTR) of Mef2d were chemically synthesized, cloned into the pScheck-2 luciferase reporter plasmid (BGI, China) and named Mef2d 3' UTR WT (wild type) and Mef2d 3' UTR Mut (mutant). Then,



500 ng Mef2d 3' UTR WT or Mef2d 3' UTR Mut and 25 nM miR-32 mimics or NC (RiboBio Co. Ltd.,China) were mixed with Lipofectamine 3000 and then transfected into RAW264.7 cells. The cells were cultured at 37 °C and 5% CO₂ for 48 h. After the cells were harvested, a luciferase assay was performed using the Dual-Luciferase Reporter Assay System Kit (Promega, San Luis Obispo, CA, USA) at Turner BioSystems (Sunnyvale, CA, USA).

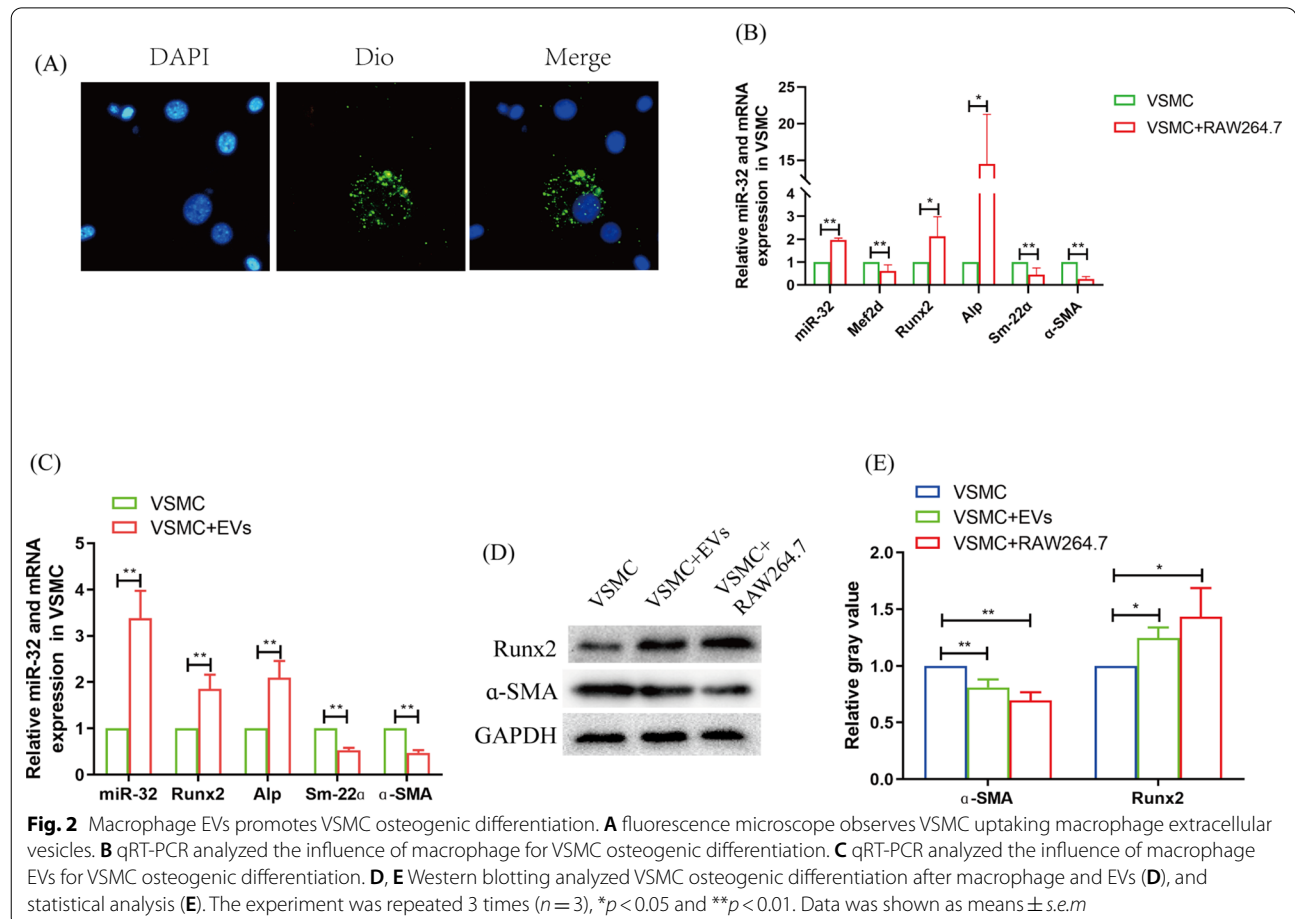
Flow cytometry

Peripheral blood or RAW264.7 cells were divided into three groups (50 µl/sample): blank group, isotype control group and experimental. The isotype control group received Rat IgG2a Kappa-FITC, Rat IgG2b Kappa-PerCP-Cy5.5, and Rat IgG2a Kappa-APC. The experimental group received CD86 monoclonal antibody-FITC, CD11b monoclonal antibody-PerCP-Cy5.5 and F4/80

monoclonal antibody-APC. All groups were incubated at room temperature for 30 min. If the sample was peripheral blood, a treatment step was added for incubation with 1 ml red blood cell lysate (BD Biosciences) for 10 min. Then, the samples were resuspended in 1 ml PBS and concentrated at 250 g for 5 min. Finally, the pellet was resuspended in 300 µl PBS and detected using BD FACS Aria™ II. The antibodies information was showed in Table 2.

RNA extraction and cDNA synthesis

Total RNA from cells or tissues was extracted using the RNA simple Total RNA Kit (TianGen Biotech (Beijing) Co., Ltd., China) or the miRNA Purification Kit (CWBio, Beijing, China), Total cDNA was synthesized using the Revert Aid First Strand cDNA Synthesis Kit (Thermo), and miRNA was synthesized using the Mir-X™ miRNA First Strand Synthesis Kit (Takara Biomedical Technology (Beijing) Co., Ltd. Beijing, China).



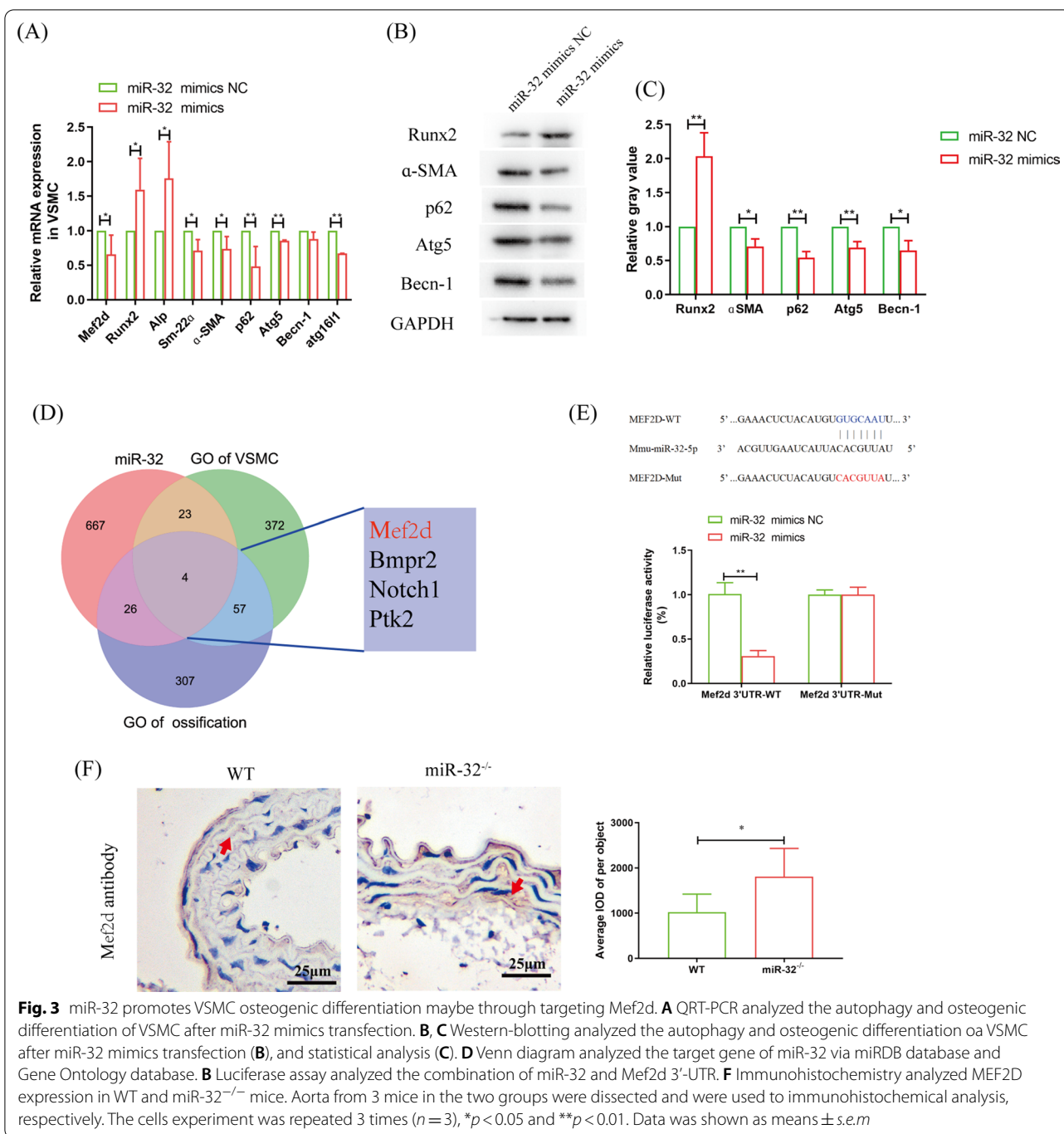


Fig. 3 miR-32 promotes VSMC osteogenic differentiation maybe through targeting Mef2d. **A** QRT-PCR analyzed the autophagy and osteogenic differentiation of VSMC after miR-32 mimics transfection. **B, C** Western-blotting analyzed the autophagy and osteogenic differentiation oa VSMC after miR-32 mimics transfection (**B**), and statistical analysis (**C**). **D** Venn diagram analyzed the target gene of miR-32 via miRDB database and Gene Ontology database. **E** Luciferase assay analyzed the combination of miR-32 and Mef2d 3'-UTR. **F** Immunohistochemistry analyzed MEF2D expression in WT and miR-32^{-/-} mice. Aorta from 3 mice in the two groups were dissected and were used to immunohistochemical analysis, respectively. The cells experiment was repeated 3 times (n = 3), *p < 0.05 and **p < 0.01. Data was shown as means ± s.e.m

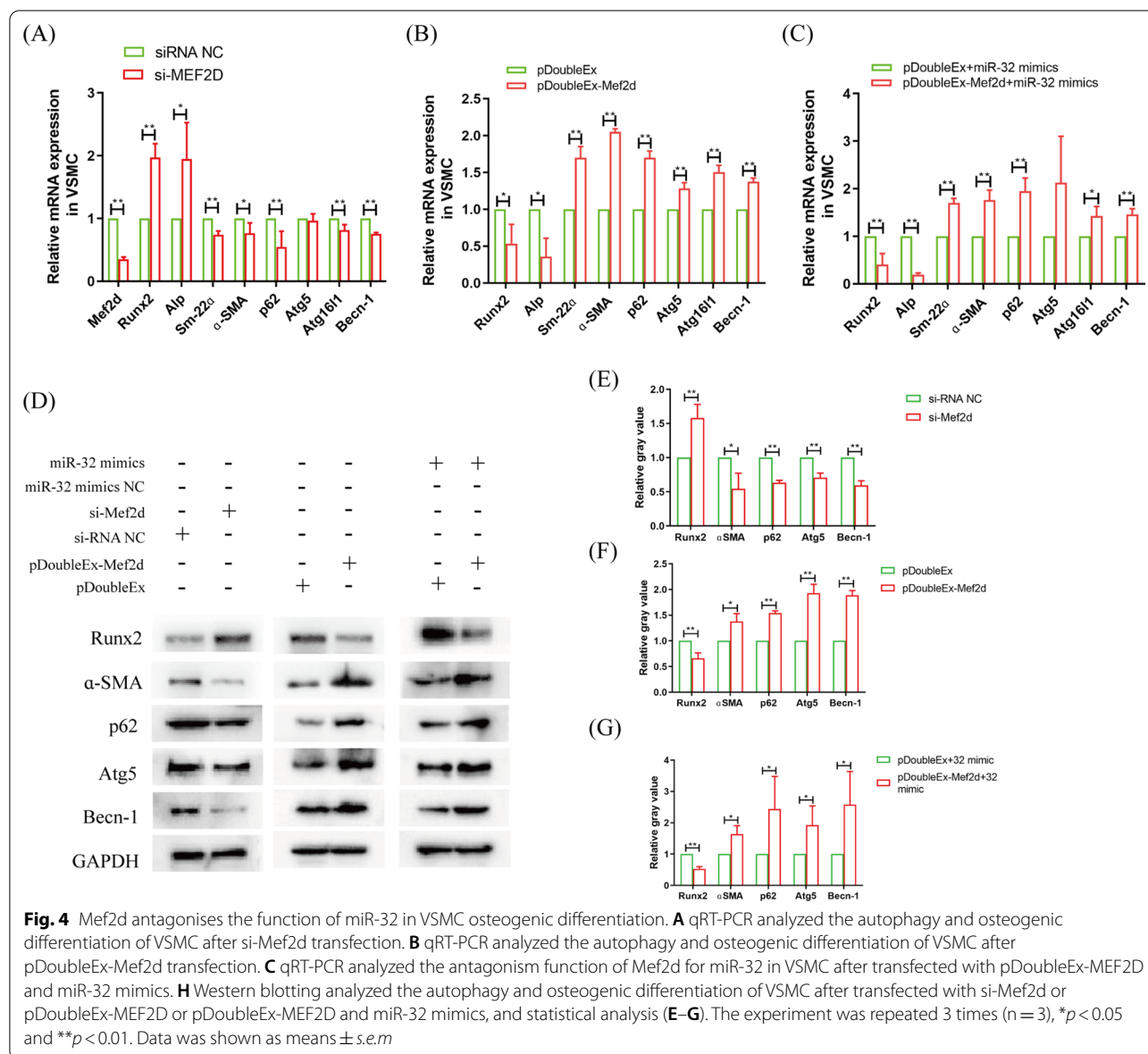
qRT-PCR

The 20 µl reaction volume of qRT-PCR contained 10 µl 2 × SYBR Green PCR Mastermix (Takara), 1 µl forward primer, and 1 µl reverse primer (Table 1), 1 µl cDNA template and 7 µl ddH₂O. The reaction program was as follows: 95 °C for 2 min; 40 cycles at 95 °C for 15 s, and 60 °C for 30 s. The experiment was performed in a LightCycler 480 II. GAPDH is used as internal

reference gene, and the results were calculated with the formula: 2^{-ΔΔCt}.

Western blotting

Protein samples were separated by SDS-PAGE, and an 8% separation gel was prepared and electrophoresed at 80 V for 20 min, followed by 120 V for 90 min. Then,

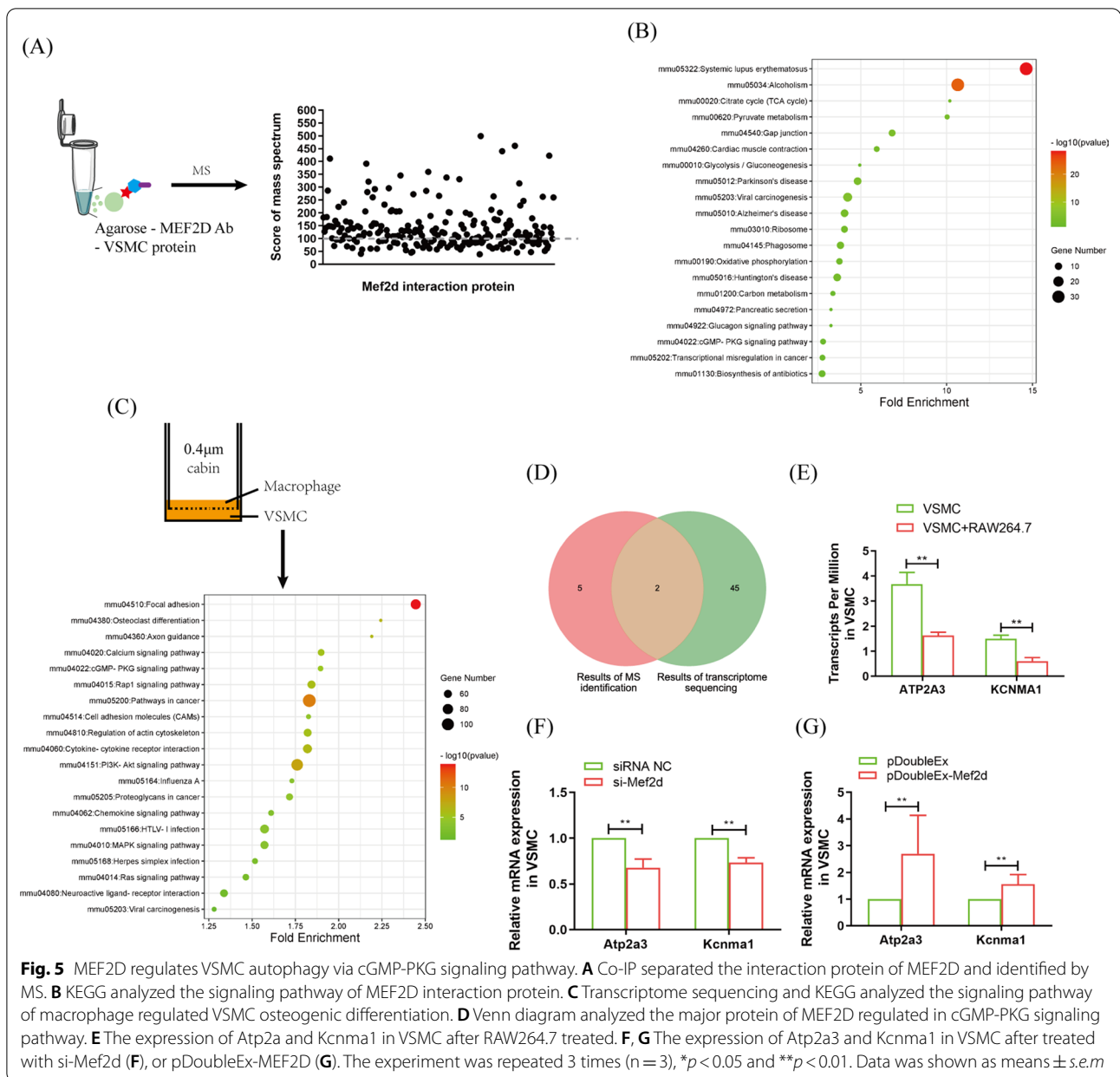


the protein was transferred onto a polyvinylidene fluoride (PVDF) membrane using a semi-dry transfer apparatus (Bio-Rad Laboratories, Inc., CA, USA) according to the manufacturer’s instructions. The membrane was then blocked at room temperature for 1 h in blocking buffer (TBS containing 5% nonfat powdered milk and 0.1% Tween-20), and then incubated with primary antibody overnight at 4 °C. After the membrane was washed 3 times for 5 min each, it was incubated with secondary antibody linked horseradish peroxidase at room temperature for 40 min and washed 2 times for 20 min each. Finally, the membrane was developed using an Immobilon Western Chemiluminescent HRP Substrate kit (EMD Millipore Corporation, MA, USA) and analyzed

using ChemiDoc™ XRS+ (Bio-Rad). The antibodies information was showed in Table 2.

Bioinformatics analysis

Cytoscape 3.7.1 software was used to search for the interacting proteins of MEF2D. The DAVID database was used for gene-annotation enrichment analysis (<https://david.ncifcrf.gov/summary.jsp>). The Gene Ontology database was used to search for gene annotation (<http://geneontology.org/>). The miRDB database was used to search the for genes of miR-32 (<https://www.mirbase.org/>). Venn diagram analysis was used to



identify the common genes (<https://bioinfogp.cnb.csic.es/tools/venny/index.html>).

Statistical analysis

All experiments were repeated at least 3 times. The data was analyzed using GraphPad Prism 7.00 software, and the results are shown as the mean \pm s.e.m. Student's t test or one-way ANOVA with Bonferroni correction was used to assess statistical significance. Multiparameter analysis of clinical data was performed using logistic

regression analysis. $p < 0.05$ or $p < 0.01$ were considered significant or very significant, respectively.

Results

Macrophage EVs promoted VSMC osteogenic differentiation under high glucose conditions

Under high glucose conditions, macrophages preferentially polarized to the M1 phenotype (Fig. 1A, B), and miR-32 expression was significantly higher than that under normal glucose conditions (Fig. 1C). Interestingly, we found that miR-32 expression was upregulated in

macrophage EVs under high glucose condition compared with normal glucose conditions (Fig. 1C). To further illustrate whether macrophages regulate VSMC biofunction through the EVs pathway, EVs from macrophages were extracted and identified (Fig. 1D–G). Macrophage EVs had a diameter of 130.1 ± 36.2 nm (Fig. 1D) and a typical membrane structure (Fig. 1E). They expressed the marker genes of EVs TSG101 and CD63 (Fig. 1F). EVs can be taken up by VSMCs (Fig. 1H). These findings suggest that EVs may be an important pathway for the communication between macrophages and VSMCs.

Furthermore, VSMCs can take up macrophage extracellular vesicles in a transwell assay with a 0.4 μ m pore membrane (Fig. 2A). After VSMCs were cocultured with RAW264.7, the marker genes of calcification, runt-related transcription factor 2 (Runx2) and alkaline phosphatase (Alp), increased significantly; the marker genes of SMC, smooth muscle 22-alpha (Sm-22a) and alpha-smooth muscle actin (α -SMA), decreased significantly (Fig. 2B, D, E). Interestingly, the results were replicated after VSMCs were treated with EVs secreted by macrophages in high glucose (Fig. 2C–E). These findings suggest that EVs promote VSMC osteogenic differentiation.

miR-32 in macrophage EVs inhibited VSMC autophagy and promoted its osteogenic differentiation

Our teams found that miR-32 is a multifunction molecule that is tightly related to cardiovascular diseases [7]. miR-32 was also increased in VSMCs after coculture with macrophages or treated with EVs secreted by macrophage under high glucose condition (Fig. 2B, C). After VSMCs were transfected with miR-32 mimics, the calcification marker genes (Runx2 and Alp) were significantly increased, and the marker genes of SMCs (Sm-22a and α -SMA) and autophagy (p62, Atg5, Becn-1 and Atg16l1) were all significantly decreased (Fig. 3A–C). These results suggest that EVs miR-32 plays an important role in the process of macrophage-promoted VSMC osteogenic differentiation.

Mef2d antagonized the function of miR-32 in VSMCs

Furthermore, we analysed the target gene of miR-32 in VSMC osteogenic differentiation. Based on the miRDB database and Gene Ontology database, we found that

Table 1 Primers sequence

Gene name	Primer sequence (5'→3')
miR-32	CGCGCTATTGCACATTACTAAGTTGCA
Mef2d-F	GGCTGGCACTAGGCAATGTAC
Mef2d-R	CTGCTGTGGCTGTGGCTGTG
iNOS-F	ACTCAGCCAAAGCCCTCACCTAC
iNOS-R	TCCAATCTCTGCCTATCCGTCTCG
TNF α -F	GCGACGTGGAAGTGGCAGAAG
TNF α -R	GCCACAAGCAGGAATGAGAAGAGG
p62-F	AGGAGGAGACGATGACTGGACAC
p62-R	TTGGTCTGTAGGAGCCTGGTGAG
Atg5-F	TGCGGTTGAGGCTCAGTTTATGTC
Atg5-R	GTCCCATCCAGAGCTGCTTGTG
Becn-1-F	AGGCAGTGGCGGCTCCTATTC
Becn-1-R	TGAGGACACCCAGGCAAGACC
Atg16l1-F	CAAGCCGAATCTGGACTGTGGATG
Atg16l1-R	CGGTCGTGACTTCTGAGACAATC
Runx2-F	AGTCCCAACTTCTGTGTCT
Runx2-R	CTGCTCCGTTCTCAAAGTGG
Bglap1-F	CAAGCAGGAGGCAATAAGGTAGTG
Bglap1-R	CATACTGGTCTGATAGCTCGTACAAG
Alp-F	CACGGCGTCCATGAGCAGAAC
Alp-R	CAGGCACAGTGGTCAAGTTGG
SM22a-F	GCCTGAGAACCCACCCCT
SM22a-R	CGAAACCCGTCAAACCCG
α SMA-F	GGCATCCACGAAACACCTAT
α SMA-R	ATGAGACAGACCTAGCCACCCG
GAPDH-F	TGTTTCTCTCGTCCCGTAG
GAPDH-R	CAATCTCCACTTTGCCACT

Mef2d was the proper target gene (Fig. 3D), and a luciferase assay verified that miR-32 mimics transfection can significantly inhibited luciferase activation in the Mef2d 3' UTR-WT group (Fig. 3E). In vitro, miR-32 mimics transfection significantly inhibited MEF2D expression in VSMCs (Fig. 3A); In vivo, we found that the expression of Mef2d was significantly increased in miR-32^{-/-} mice compared with WT mice (Fig. 3F).

Next, the roles of Mef2d were analysis in the process of VSMC autophagy and osteogenic differentiation were analysed. After VSMCs were transfected with si-Mef2d, the marker genes of calcification (Runx2 and Alp) were all significantly increased, and the marker genes of SMCs

(See figure on next page.)

Fig. 6 In vivo analysis of macrophage EVs miR-32 promotes aorta calcification by inhibited autophagy. Analysis of VSMC autophagy and osteogenic differentiation in the aorta of miR-32^{-/-} T2D mice after treated with macrophage EVs. **A** Blood glucose analysis. **B** IPITT analysis. **C** HOMA-IR analysis. **D** Immunohistochemistry analyzed miR-32 expression in aorta of miR-32^{-/-} mice, and WT mice, and miR-32^{-/-} injection EVs. **C** qRT-PCR analyzed aorta osteogenic differentiation. **F, G** alizarin red staining analyzed aorta calcification after macrophage EVs injection (**F**), and statistical analysis (**G**). **H–K** Immunofluorescence analyzed p62 and LC3 expressions in aorta (**H**), and statistical analyzed the puncta of p62 (**I**), LC3 (**J**), and p62-LC3 (**K**). 3 per 5 mice in different groups were used in the detection. * $p < 0.05$ and ** $p < 0.01$. Data was shown as means \pm s.e.m

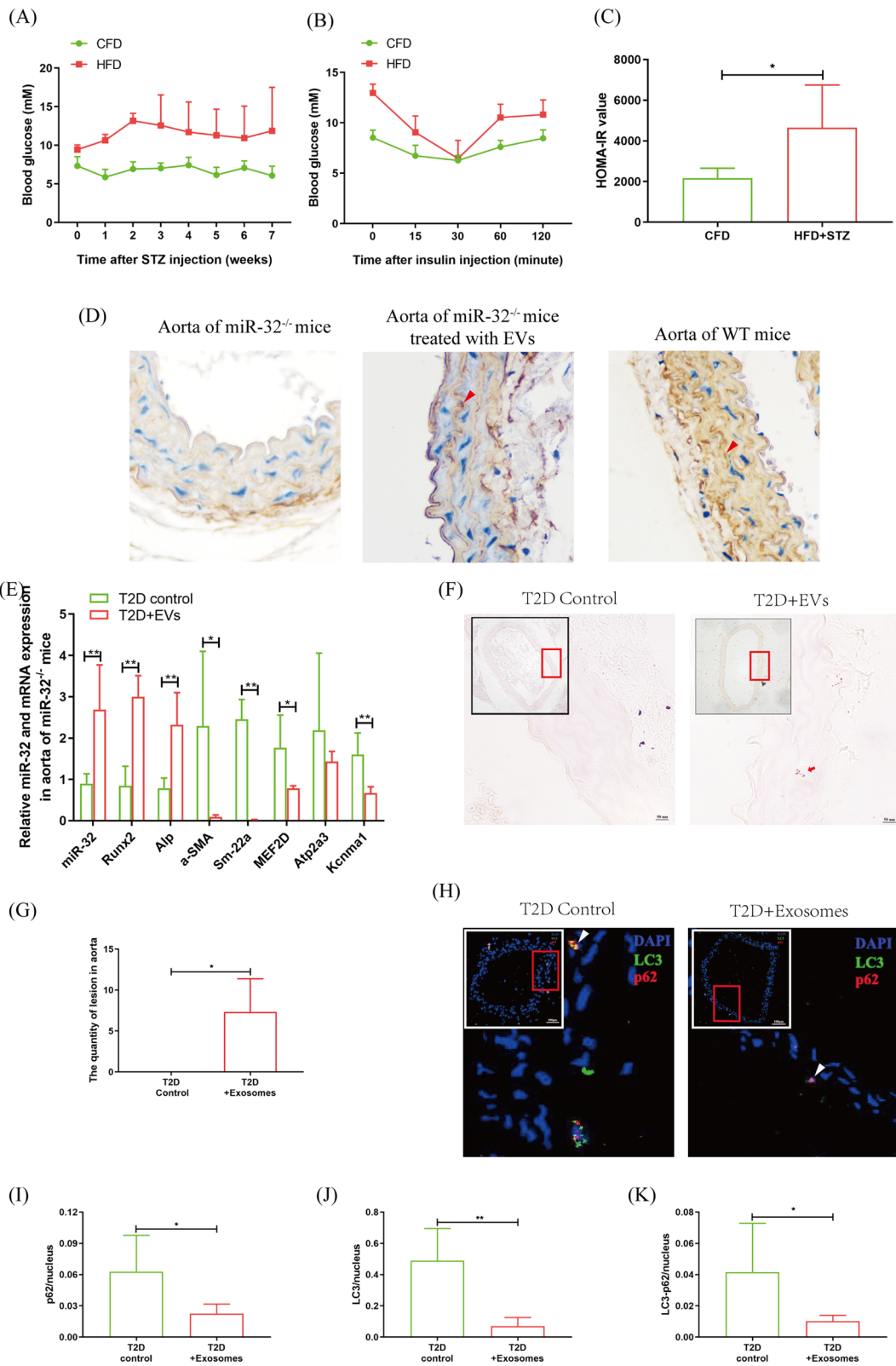


Fig. 6 (See legend on previous page.)

(Sm-22 α and α -SMA) and autophagy (p62, Atg5, Becn-1 and Atg16l1) were all significantly decreased (Fig. 4A, D, E). When VSMCs overexpressed Mef2d, the marker genes of calcification were all significantly decreased, and the marker genes of SMC and autophagy were all significantly increased (Fig. 4B, D, F). Importantly, rescue experiments confirmed that Mef2d overexpression antagonized the function of miR-32 in VSMC autophagy and osteogenic differentiation (Fig. 4C, D, G). These results suggest that miR-32 regulates VSMC autophagy and osteogenic differentiation by targeting to Mef2d.

cGMP/PKG is the key signalling pathway by which Mef2d regulates VSMC osteogenic differentiation

To reveal the mechanism by which Mef2d regulates autophagy, the proteins that interacted with Mef2d were separated using Co-IP and were identified using mass spectrometry (MS) (Fig. 5A, Additional file 1). A total of 159 proteins were identified. They were involved in 26 pathways according to DAVID cluster analysis, and 20 of them appeared to be enriched dot bubbles (Fig. 5B). In addition, VSMCs cocultured with macrophages were used for transcriptome sequencing analysis (Additional file 2). The DAVID cluster was used to analyse proteins that were significantly altered by more than twofold. In the top 20 pathways, the cGMP-PKG signalling pathway and viral carcinogenesis were the common signalling pathways regulated by Mef2d (Fig. 5B, C, Additional files 1, 2), and the cGMP-PKG signaling pathway was selected for further research due to its noticeable function in T2D-related cardiovascular diseases [27]. Then, Venn diagram was used to explore the common genes in the cGMP-PKG signalling pathway. The results revealed two common genes, ATPase sarcoplasmic/endoplasmic reticulum Ca²⁺ transporting 3 (Atp2a3) and potassium calcium-activated channel subfamily M alpha 1 (Kcnma1) (Fig. 5D). The expression trend of these two genes was consistent with that of Mef2d in VSMCs after coculture with macrophages (Fig. 5E). Moreover, pDoubleEX-MEF2D transfection promoted Atp2a3 and Kcnma1 expression in VSMCs, while si-Mef2d transfection inhibited the expression of these genes (Fig. 5F, G). These findings suggest that the cGMP-PKG signalling pathway is crucial for Mef2d regulation of VSMC autophagy.

Macrophage EVs miR-32 promoted aortic calcification by inhibiting autophagy in miR-32^{-/-} T2D mice

In vivo, miR-32^{-/-} mice were used to establish a T2D mouse model. Compared with CFD mice, the model mice had marked characteristics of T2D, such as high-blood glucose levels and insulin resistance (Fig. 6A–C). Then, the T2D mice were injected with EVs secreted by macrophages under high glucose conditions, and miR-32

appeared in the VSMCs of the aorta (Fig. 6D). Moreover, in EVs-treated miR-32^{-/-} T2D mice, the expression of miR-32 and the ossification genes (Runx2 and Alp) were all significantly increased, and the marker genes of SMCs (α -SMA and Sm-22 α) and the cGMP-PKG signalling pathway (Atp2a3 and Kcnma1) were all significantly decreased (Fig. 6E). In addition, autophagy analysis revealed that p62, LC3, and p62-LC3 puncta were all significantly decreased in the aortas of miR-32^{-/-} mice after treatment with EVs (Fig. 6F–I). These findings suggest that miR-32 is an important molecule in macrophage EVs that promotes aortic calcification in T2D mice.

Discussion

Diabetes is a chronic disease that is characterized by impaired glucose metabolism. This condition can easily cause microvascular and macrovascular complications due to high glucose levels that can easily activate the immune system [28, 29], especially the activation of macrophages [30]. Based on our previous reports on miR-32 in coronary artery calcification and microglia [7, 8], this study further explored the roles and mechanisms by which miR-32 acts in the process of macrophage-regulated T2D VC.

High glucose is one of the major pathological factors associated with diabetes [31], and it easily leads to the dysregulation of the functions of inflammatory and immune cells, including macrophages [16]. Under high glucose conditions, we found that macrophages preferentially polarized to the M1 phenotype (Fig. 1A, B). M1 macrophages constitute the primary immune cell-mediated inflammatory reaction, which is one of the leading causes of VC [32]. However, in addition to producing inflammatory factors, secreting EVs is another crucial pathway by which macrophages drive the function of immune cells [33, 34]. Furthermore, EVs are key carriers of miRNAs [35]. Interestingly, we found that high glucose conditions promoted miR-32 expression not only in macrophages but also in their EVs (Fig. 1C). Furthermore, macrophages and EVs all significantly increased miR-32 expression in VSMCs and their osteogenic differentiation (Fig. 2). Therefore, these findings suggest that macrophage EVs promote VSMC osteogenic differentiation and that miR-32 may drive the function of EVs under high-glucose conditions.

Next, we identified that Mef2d, which is involved in the autophagy process [36–38], is the key target gene of miR-32 in VSMC osteogenic differentiation (Figs. 3, 4). To illustrate the regulatory pathway of Mef2d in VSMC autophagy, we identified the protein that interacts with Mef2d and then analysed the change in transcription

Table 2 Antibodies used in the experiments

Antibody name	Source	Manufacturer	Catalog # (RRID)	Application
Anti-F4/80-APC	Rat	Thermo Fisher Scientific	17-4801-80#AB_2784647	IF(1:50)
Anti-CD11b-Percp-Cy5.5	Rat	Thermo Fisher Scientific	45-0112-80#AB_953560	IF(1:50)
Anti-CD86-FITC	Rat	Thermo Fisher Scientific	11-0862-82#AB_465148	IF(1:50)
Anti-iNOS	Rabbit	proteintech	18985-1-AP#AB_2782960	IHC(1:100)
Anti-F4/80	Rat	Thermo Fisher Scientific	14-4801-82#AB_467558	IHC(1:100)
α -SMA	Rabbit	Cell signaling	19245#AB_2734735	WB(1:1000)
Runx2	Rabbit	abcam	20700-1-AP#AB_2722783	WB(1:500)
Anti-CD63	Rabbit	Thermo Fisher Scientific	PA5-92370#AB_2806456	WB(1:1000)
Anti-TSG101	Rabbit	Thermo Fisher Scientific	PA5-82236#AB_2789397	WB(1:1000)
Anti-Mef2d	Rabbit	Proteintech	14353-1-AP#AB_2878046	WB(1:1000) IHC(1:100)
Anti-p62	Rabbit	Proteintech	18420-1-AP#AB_10694431	WB(1:1000)
Anti-p62	mouse	Proteintech	66184-1-Ig#AB_2881579	IFC(1:100)
Anti-Atg5	Rabbit	Proteintech	10181-2-AP#AB_2062045	WB(1:1000)
Anti-Becn-1	Rabbit	Proteintech	11306-1-AP#AB_2259061	WB(1:1000)
Anti-LC3	Rabbit	Proteintech	14600-1-AP#AB_2137737	IFC(1:100)

levels in VSMCs cocultured with with macrophage under high glucose conditions. Cluster analysis showed that the cGMP-PKG was the common signalling pathway, and *Ato2a3* and *Kcnma1* were the common proteins in cGMP-PKG (Fig. 5A–E). Impaired cGMP-PKG signalling causes cardiomyocyte stiffening in diabetic hearts, and the symptoms can be modulated through restoration of the normal kinase activities of PKG by neuregulin-1 [27]. In particular, cGMP-PKG is tightly correlated with diabetes vascular dysfunction and cardiomyocyte autophagy [39–41]. A reduction in autophagy leads to cardiac dysfunction, including cardiovascular calcification [42, 43]. This evidence highlights the important relationship between the cGMP-PKG signalling pathway and VSMC autophagy. Further research found that the expression of *Atp2a3* and *Kcnma1* was consistent with the expression change in *Mef2d* expression (Fig. 5E, G). Knockout of *Kcnma1* leads to autophagic dysfunction [44]. Therefore, these findings suggest that *Mef2d* mediates VSMC autophagy by regulating the cGMP-PKG signalling pathway.

EVs transplantation is typically used to analyse the function of miRNAs in cell–cell crosstalk [45]. After T2D miR-32^{-/-} mice were injected with miR-32 EVs, miR-32 appeared in the aortic (Fig. 6D), and aortic calcification was significantly increased (Fig. 6E–G). One important cause of VSMC calcification is impaired autophagy [24], and the changes in LC3, p62, and LC3-p62 dots represent autophagosome formation [46]. In this study, EVs

transplantation significantly promoted aortic calcification and inhibited autophagosome formation in the aortas of T2D miR-32^{-/-} mice (Fig. 6H–K). Thus, these findings suggest that macrophage EVs promote the development of T2D VC that miR-32 is a key regulator of this process.

Although miR-32 has been identified as an important molecule in macrophage EVs that promotes T2D VC, we cannot exclude the influence of other EVs compositions on T2D VC. Currently, some reports attempted to resolve this problem. Luo ZL et al. eliminated DNA in EVs through electroporation and DNase I treatment [47]. Therefore, the feasibility of electroporation and miRNA inhibitor treatment will promote research on EVs function.

Conclusions

Our findings demonstrated that high glucose conditions promote macrophage M1 polarization by upregulating miR-32 and increasing miR-32 levels in EVs. Furthermore, EVs miR-32 promotes aortic calcification in T2D miR-32^{-/-} mice through miR-32/*Mef2d*/cGMP-PKG-mediated VSMC autophagy. These findings illustrate an important mechanism by which macrophages promote VC in T2D and identify a candidate biomarker of T2D VC.

Supplementary Information

The online version contains supplementary material available at <https://doi.org/10.1186/s12967-022-03502-8>.

Additional file 1. MS analyze the interaction protein of *Mef2d*.

Additional file 2. Transcriptome sequencing analyze the influence of macrophage for genes expression in VSMC.

Acknowledgements

We thank Dr. Pan Qunwen from the Affiliated Hospital of Guangdong Medical University for assistance with nanoparticle tracking analysis

Author contributions

Laboratory experiments, data analysis and manuscript writing were accomplished by JC; part of experimental design and data analysis were accomplished by CC and QC; part of experiment were accomplished by YG, ZZ, AL and SY; Animal's feeding was accomplished by JC, CC, QY and YH; guidance of experimental design and manuscript writing was accomplished by XZ and JL. All authors have read and approved the final manuscript.

Funding

This work was supported by the National Natural Science Foundation of China (No. 81873651); Natural Science Foundation of Hunan Province, China (No. 2020SK2107, No. 2021JJ40490 and No. 2021JJ70113); Scientific Research Fund Project of Hunan Provincial Health Commission, China (No. 20201981 and No. 20201901).

Availability of data and materials

All data in the article can be requested from the corresponding author.

Declarations

Ethics approval and consent to participate

This research was approved by the Animal Welfare and Research Ethics Committee of the Institute of University of South China.

Consent for publication

Not applicable.

Competing interests

The authors declare that the research was conducted in the absence of any commercial or financial relationships that could be construed as a potential conflict of interest.

Author details

¹The First Affiliated Hospital, Institute of Clinical Medicine, Department of Endocrinology and Metabolism, Hengyang Medical School, University of South China, Hengyang 421000, Hunan, China. ²The First Affiliated Hospital, Department of Laboratory Medicine, Hengyang Medical School, University of South China, Hengyang 421000, China. ³The First Affiliated Hospital, Institute of Clinical Medicine, Department of Tumor Research, Hengyang Medical School, University of South China, Hengyang 421000, China.

Received: 28 April 2022 Accepted: 24 June 2022

Published online: 06 July 2022

References

- Gu M, Mordwinkin NM, Kooreman NG, Lee J, Wu H, Hu S, et al. Pravastatin reverses obesity-induced dysfunction of induced pluripotent stem cell-derived endothelial cells via a nitric oxide-dependent mechanism. *Eur Heart J*. 2015;36(13):806–16. <https://doi.org/10.1093/eurheartj/ehu411>.
- Mauricio D, Alonso N, Gratacòs M. Chronic diabetes complications: the need to move beyond classical concepts. *Trends Endocrinol Metab*. 2020;31(4):287–95. <https://doi.org/10.1016/j.tem.2020.01.007>.
- Nakahara T, Dweck MR, Narula N, Pisapia D, Narula J, Strauss HW. Coronary artery calcification: from mechanism to molecular imaging. *JACC Cardiovasc Imaging*. 2017;10(5):582–93. <https://doi.org/10.1016/j.jcmg.2017.03.005>.
- Leopold JA. Vascular calcification: mechanisms of vascular smooth muscle cell calcification. *Trends Cardiovasc Med*. 2015;25(4):267–74. <https://doi.org/10.1016/j.tcm.2014.10.021>.
- Jia S, Ma WD, Zhang CY, Zhang Y, Yao ZH, Quan XH, et al. Tanshinone IIA attenuates high glucose induced human VSMC proliferation and migration through miR-21-5p-mediated tropomyosin 1 downregulation. *Arch Biochem Biophys*. 2019;677: 108154. <https://doi.org/10.1016/j.abb.2019.108154>.
- Hao W, Yang R, Yang Y, Jin S, Li Y, Yuan F, et al. Stellate ganglion block ameliorates vascular calcification by inhibiting endoplasmic reticulum stress. *Life Sci*. 2018;193:1–8. <https://doi.org/10.1016/j.lfs.2017.12.002>.
- Liu J, Xiao X, Shen Y, Chen L, Xu C, Zhao H, et al. MicroRNA-32 promotes calcification in vascular smooth muscle cells: implications as a novel marker for coronary artery calcification. *PLoS ONE*. 2017;12(3): e0174138. <https://doi.org/10.1371/journal.pone.0174138>.
- Cao J, Chen L, Zhong X, Shen Y, Gao Y, Chen Q, et al. miR32-5p promoted vascular smooth muscle cell calcification by upregulating TNF α in the microenvironment. *BMC Immunol*. 2020;21(1):3. <https://doi.org/10.1186/s12865-019-0324-x>.
- Liu B, Deng X, Jiang Q, Li G, Zhang J, Zhang N, et al. Scoparone improves hepatic inflammation and autophagy in mice with nonalcoholic steatohepatitis by regulating the ROS/P38/Nrf2 axis and PI3K/AKT/mTOR pathway in macrophages. *Biomed Pharmacother Biomed Pharmacother*. 2020;125:109895. <https://doi.org/10.1016/j.biopha.2020.109895>.
- Ensan S, Li A, Besla R, Degousee N, Cosme J, Roufaiel M, et al. Self-renewing resident arterial macrophages arise from embryonic CX3CR1(+) precursors and circulating monocytes immediately after birth. *Nat Immunol*. 2016;17(2):159–68. <https://doi.org/10.1038/ni.3343>.
- Winkels H, Ehinger E, Vassallo M, Buscher K, Dinh HQ, Kobiyama K, et al. Atlas of the immune cell repertoire in mouse atherosclerosis defined by single-cell RNA-sequencing and mass cytometry. *Circ Res*. 2018;122(12):1675–88. <https://doi.org/10.1161/circresaha.117.312513>.
- Fernandez DM, Rahman AH, Fernandez NF, Chudnovskiy A, Amir ED, Amadori L, et al. Single-cell immune landscape of human atherosclerotic plaques. *Nat Med*. 2019;25(10):1576–88. <https://doi.org/10.1038/s41591-019-0590-4>.
- Feldmann K, Grandoch M, Kohlmorgen C, Valentin B, Gerfer S, Nagy N, et al. Decreased M1 macrophage polarization in dabigatran-treated Ldlr-deficient mice: implications for atherosclerosis and adipose tissue inflammation. *Atherosclerosis*. 2019;287:81–8. <https://doi.org/10.1016/j.atherosclerosis.2019.06.897>.
- New SE, Goettsch C, Aikawa M, Marchini JF, Shibasaki M, Yabusaki K, et al. Macrophage-derived matrix vesicles: an alternative novel mechanism for microcalcification in atherosclerotic plaques. *Circ Res*. 2013;113(1):72–7. <https://doi.org/10.1161/circresaha.113.301036>.
- Jha AK, Huang SC, Sergushichev A, Lampropoulou V, Ivanova Y, Loginicheva E, et al. Network integration of parallel metabolic and transcriptional data reveals metabolic modules that regulate macrophage polarization. *Immunity*. 2015;42(3):419–30. <https://doi.org/10.1016/j.immuni.2015.02.005>.
- Huang SM, Wu CS, Chiu MH, Wu CH, Chang YT, Chen GS, et al. High glucose environment induces M1 macrophage polarization that impairs keratinocyte migration via TNF- α : An important mechanism to delay the diabetic wound healing. *J Dermatol Sci*. 2019;96(3):159–67. <https://doi.org/10.1016/j.jdermsci.2019.11.004>.
- Wang Y, Xie Y, Zhang A, Wang M, Fang Z, Zhang J. Exosomes: an emerging factor in atherosclerosis. *Biomed Pharmacother Biomed Pharmacother*. 2019;115:108951. <https://doi.org/10.1016/j.biopha.2019.108951>.
- Théry C, Witwer KW, Aikawa E, Alcaraz MJ, Anderson JD, Andriantsitohaina R, et al. Minimal information for studies of extracellular vesicles 2018 (MISEV2018): a position statement of the International Society for Extracellular Vesicles and update of the MISEV2014 guidelines. *J Extracell Vesicles*. 2018;7(1):1535750. <https://doi.org/10.1080/20013078.2018.1535750>.
- Mizushima N, Yoshimori T, Ohsumi Y. The role of Atg proteins in autophagosome formation. *Annu Rev Cell Dev Biol*. 2011;27:107–32. <https://doi.org/10.1146/annurev-cellbio-092910-154005>.
- Xie Z, Klionsky DJ. Autophagosome formation: core machinery and adaptations. *Nat Cell Biol*. 2007;9(10):1102–9. <https://doi.org/10.1038/ncb1007-1102>.
- Nakatogawa H. Two ubiquitin-like conjugation systems that mediate membrane formation during autophagy. *Essays Biochem*. 2013;55:39–50. <https://doi.org/10.1042/bse0550039>.

22. Shaid S, Brandts CH, Serve H, Dikic I. Ubiquitination and selective autophagy. *Cell Death Differ*. 2013;20(1):21–30. <https://doi.org/10.1038/cdd.2012.72>.
23. Banday MZ, Sameer AS, Nissar S. Pathophysiology of diabetes: an overview. *Avicenna J Med*. 2020;10(4):174–88. https://doi.org/10.4103/ajm.ajm_53_20.
24. Ni T, Gao F, Zhang J, Lin H, Luo H, Chi J, et al. Impaired autophagy mediates hyperhomocysteinemia-induced HA-VSMC phenotypic switching. *J Mol Histol*. 2019;50(4):305–14. <https://doi.org/10.1007/s10735-019-09827-x>.
25. Grootaert MOJ, Moulis M, Roth L, Martinet W, Vindis C, Bennett MR, et al. Vascular smooth muscle cell death, autophagy and senescence in atherosclerosis. *Cardiovasc Res*. 2018;114(4):622–34. <https://doi.org/10.1093/cvr/cvy007>.
26. Morciano G, Patergnani S, Pedriali G, Cimaglia P, Mikus E, Calvi S, et al. Impairment of mitophagy and autophagy accompanies calcific aortic valve stenosis favoring cell death and the severity of disease. *Cardiovasc Res*. 2021. <https://doi.org/10.1093/cvr/cvab267>.
27. Hopf AE, Andresen C, Kötter S, Isic M, Ulrich K, Sahin S, et al. Diabetes-induced cardiomyocyte passive stiffening is caused by impaired insulin-dependent titin modification and can be modulated by neuregulin-1. *Circ Res*. 2018;123(3):342–55. <https://doi.org/10.1161/circresaha.117.312166>.
28. Adeshara KA, Bangar NS, Doshi PR, Diwan A, Tupe RS. Action of metformin therapy against advanced glycation, oxidative stress and inflammation in type 2 diabetes patients: 3 months follow-up study. *Diabetes Metab Syndr*. 2020;14(5):1449–58. <https://doi.org/10.1016/j.dsx.2020.07.036>.
29. Edgar L, Akbar N, Braithwaite AT, Krausgruber T, Gallart-Ayala H, Bailey J, et al. Hyperglycaemia induces trained immunity in macrophages and their precursors and promotes atherosclerosis. *Circulation*. 2021. <https://doi.org/10.1161/circulationaha.120.046464>.
30. Zhang Q, Wang J, Yadav DK, Bai X, Liang T. Glucose metabolism: the metabolic signature of tumor associated macrophage. *Front Immunol*. 2021;12:702580–702580. <https://doi.org/10.3389/fimmu.2021.702580>.
31. Tanwar VS, Reddy MA, Natarajan R. Emerging role of long non-coding RNAs in diabetic vascular complications. *Front Endocrinol*. 2021;12:665811. <https://doi.org/10.3389/fendo.2021.665811>.
32. Lee SJ, Lee I-K, Jeon J-H. Vascular calcification-new insights into its mechanism. *Int J Mol Sci*. 2020;21(8):2685. <https://doi.org/10.3390/ijms21082685>.
33. Jansen F, Li Q, Pfeifer A, Werner N. Endothelial- and immune cell-derived extracellular vesicles in the regulation of cardiovascular health and disease. *JACC Basic Transl Sci*. 2017;2(6):790–807. <https://doi.org/10.1016/j.jacbts.2017.08.004>.
34. Juzenas S, Venkatesh G, Hübenthal M, Hoepfner MP, Du ZG, Paulsen M, et al. A comprehensive, cell specific microRNA catalogue of human peripheral blood. *Nucleic Acids Res*. 2017;45(16):9290–301. <https://doi.org/10.1093/nar/gkx706>.
35. Kim DK, Bandara G, Cho YE, Komarow HD, Donahue DR, Karim B, et al. Mastocytosis-derived extracellular vesicles deliver miR-23a and miR-30a into pre-osteoblasts and prevent osteoblastogenesis and bone formation. *Nat Commun*. 2021;12(1):2527. <https://doi.org/10.1038/s41467-021-22754-4>.
36. Yang Q, Mao Z. The complexity in regulation of MEF2D by chaperone-mediated autophagy. *Autophagy*. 2009;5(7):1073–4. <https://doi.org/10.4161/auto.5.7.9824>.
37. Gao L, She H, Li W, Zeng J, Zhu J, Jones DP, et al. Oxidation of survival factor MEF2D in neuronal death and Parkinson's disease. *Antioxid Redox Signal*. 2014;20(18):2936–48. <https://doi.org/10.1089/ars.2013.5399>.
38. Sala G, Marinig D, Arosio A, Ferrarese C. Role of chaperone-mediated autophagy dysfunctions in the pathogenesis of Parkinson's disease. *Front Mol Neurosci*. 2016;9:157. <https://doi.org/10.3389/fnmol.2016.00157>.
39. Meakin PJ, Coull BM, Tuharska Z, McCaffery C, Akoumianakis I, Antoniadou C, et al. Elevated circulating amyloid concentrations in obesity and diabetes promote vascular dysfunction. *J Clin Investig*. 2020;130(8):4104–17. <https://doi.org/10.1172/jci122237>.
40. Zhao XX, Cho H, Lee S, Woo JS, Song MY, Cheng XW, et al. BAY60-2770 attenuates doxorubicin-induced cardiotoxicity by decreased oxidative stress and enhanced autophagy. *Chem Biol Interact*. 2020;328: 109190. <https://doi.org/10.1016/j.cbi.2020.109190>.
41. Coliva G, Duarte S, Pérez-Sala D, Fedorova M. Impact of inhibition of the autophagy-lysosomal pathway on biomolecules carbonylation and proteome regulation in rat cardiac cells. *Redox Biol*. 2019;23: 101123. <https://doi.org/10.1016/j.redox.2019.101123>.
42. Fan Y, Shao J, Wei S, Song C, Li Y, Jiang S. Self-eating and heart: the emerging roles of autophagy in calcific aortic valve disease. *Aging Dis*. 2021;12(5):1287–303. <https://doi.org/10.14336/ad.2021.0101>.
43. Lu Y, Yuan T, Min X, Yuan Z, Cai Z. AMPK: potential therapeutic target for vascular calcification. *Front Cardiovasc Med*. 2021;8: 670222. <https://doi.org/10.3389/fcvm.2021.670222>.
44. Yao Y, Qu D, Jing X, Jia Y, Zhong Q, Zhuo L, et al. Molecular mechanisms of epileptic encephalopathy caused by KCNMA1 loss-of-function mutations. *Front Pharmacol*. 2021;12: 775328. <https://doi.org/10.3389/fphar.2021.775328>.
45. Castaño C, Kalko S, Novials A, Párrizas M. Obesity-associated exosomal miRNAs modulate glucose and lipid metabolism in mice. *Proc Natl Acad Sci USA*. 2018;115(48):12158–63. <https://doi.org/10.1073/pnas.1808855115>.
46. Nakamura A, Kurihara S, Takahashi D, Ohashi W, Nakamura Y, Kimura S, et al. Symbiotic polyamine metabolism regulates epithelial proliferation and macrophage differentiation in the colon. *Nat Commun*. 2021;12(1):2105. <https://doi.org/10.1038/s41467-021-22212-1>.
47. Luo Z, Ji Y, Gao H, Gomes Dos Reis FC, Bandyopadhyay G, Jin Z, et al. CRlg(+) macrophages prevent gut microbial DNA-containing extracellular vesicle-induced tissue inflammation and insulin resistance. *Gastroenterology*. 2021;160(3):863–74. <https://doi.org/10.1053/j.gastro.2020.10.042>.

Publisher's Note

Springer Nature remains neutral with regard to jurisdictional claims in published maps and institutional affiliations.

Ready to submit your research? Choose BMC and benefit from:

- fast, convenient online submission
- thorough peer review by experienced researchers in your field
- rapid publication on acceptance
- support for research data, including large and complex data types
- gold Open Access which fosters wider collaboration and increased citations
- maximum visibility for your research: over 100M website views per year

At BMC, research is always in progress.

Learn more biomedcentral.com/submissions

